

Improved Site-Specific Numerical Prediction of Fog and Low Clouds: A Feasibility Study

THIERRY BERGOT, DOMINIQUE CARRER,* JOËL NOILHAN, AND PHILIPPE BOUGEAULT[†]

Centre National de Recherches Météorologiques, Météo-France, Toulouse, France

(Manuscript received 25 March 2004, in final form 18 January 2005)

ABSTRACT

Accurate short-term forecasts of low ceiling and visibility are vital to air traffic operation, in order to maximize the use of an airport. The research presented here uses specific local observations and a detailed numerical 1D model in an integrated approach. The goal of the proposed methodology is to improve the local prediction of poor visibility and low clouds at Paris's Charles de Gaulle International Airport. In addition to the development of an integrated observations and model-based forecasting system, this study will try to assess whether or not the increased local observing network yields improvements in short-term forecasts of low ceiling and poor visibility. Tests have been performed in a systematic manner during 5 months (the 2002/03 winter season). Encouraging results show that the inclusion of dedicated observations into the local 1D forecast system provides significant improvement to the forecast. Inspection of events indicates that the improvement in very short-term forecasts is a consequence of the ability of the forecast system to more accurately characterize the boundary layer processes, especially during night. Accurate forecast of low cloud seems more difficult since it strongly depends on the 3D mesoscale flow. This study also demonstrates that the use of a 1D model to forecast fogs and low clouds could only be beneficial if it is associated with local measurements and with a local assimilation scheme. The assimilation procedure used in this study is based on different steps: in the first step the atmospheric profiles are estimated in a one-dimensional variational data assimilation (1DVAR) framework, in the second step these atmospheric profiles are modified when fog and/or low clouds are detected, and in the third step the soil profiles are estimated in order to keep the consistency between the soil state and atmospheric measurements.

1. Introduction

The prediction of cloud ceiling and visibility near the surface is a formidable challenge for the operational weather forecast services. Air traffic safety and operational efficiency depend heavily upon accurate and timely forecasts of these atmospheric conditions. Adverse ceiling and visibility conditions can strongly reduce the efficiency of terminal area traffic flow, and for example, at Paris's Charles de Gaulle International Airport (Paris-CDG), the capacity of landing and take-off is reduced by a factor of 2 when the visibility is less

than 600 m or when the ceiling is less than 200 ft [~ 60 m; low visibility procedures (LVP) conditions]. The occurrence of low ceilings and/or poor visibility conditions restricting the flow of air traffic into major airport terminals is one of the major causes of aircraft delay.

In recent years, efforts have been made to improve the forecast of ceiling and visibility around airports. Unfortunately current operational NWP models may not be able to provide enough valuable information, which would be useful in improving short-term ceiling and visibility predictions. The lack of accurate ceiling and visibility forecasts is the results of a variety of factors including the following:

- Quality forecasts are dependent upon having a higher density and dedicated observing network that can supply detailed information (e.g., radiative fluxes, vertical stability of the atmosphere, horizontal gradient of humidity). This high-density observing network has to be associated with a mesoscale assimilation scheme in order to create accurate initial condi-

* Current affiliation: DP/CNMA, Météo-France, Taverny, France.

[†] Current affiliation: ECMWF, Reading, United Kingdom.

Corresponding author address: T. Bergot, CNRM/GMME, Météo-France, 42, Ave. G. Coriolis, F-31057 Toulouse Cedex, France.

E-mail: Thierry.Bergot@meteo.fr

tions. In many cases, this information is currently not available.

- A thorough understanding of the physical processes associated with fog and low clouds (interaction between turbulence processes—specifically in stable cases—microphysics and radiation) has not yet been achieved. Research on physical processes involved in the fog and low clouds needs to continue.
- Although advancements in numerical modeling have been substantial over the past decade, considerable research and development is necessary to reach a state where the operational NWP models can resolve the evolution of the atmosphere under cloudy conditions, in particular in cases of low cloud and fog.

In an attempt to overcome these deficiencies, the research presented herein integrates dedicated observations and up-to-date numerical models.

Although fog and low clouds can be formed for a variety of reasons, it is apparent that the land surface and boundary layer processes play a fundamental role in the onset and evolution of these clouds. Given the strong vertical gradient frequently observed in the nocturnal boundary layer, a high vertical resolution model is necessary to forecast the boundary layer structure and consequently the ceiling and visibility. Preliminary results on the impact of the vertical resolution in the numerical forecasting of fog and low cloud can be found in Tardif (2004). However, it is not currently possible to run a 3D mesoscale model operationally with very high vertical resolution in order to have numerous levels inside the fog layer (on the order of 50 m). One way to resolve this problem is to use a one-dimensional (1D) model, with high vertical resolution, forced with the mesoscale tendencies provided by operational numerical weather forecasts models. This idea has been successfully employed by Musson-Genon (1987) and Bergot and Guedalia (1994) to reproduce the nocturnal boundary layer and the onset and evolution of fog. For this study, we use the atmospheric 1D Code de Brouillard à l'Echelle Locale [COBEL; developed in collaboration between the Laboratoire d'Aérodynamique—Université Paul Sabatier/Centre National de la Recherche Scientifique (CNRS) and Météo-France/Centre National de Recherches Météorologiques (CNRM)] model, which has been developed to study the boundary layer and fog at the local scale (Guedalia and Bergot 1994; Bergot and Guedalia 1996).

The capabilities exhibited by the COBEL model during these previous studies suggest that it is able to predict the evolution of the lower atmosphere and, especially, of the fog layer. Nevertheless, phenomena such

as fog and low clouds are closely coupled to the exchanges between the surface and the atmosphere. Siebert et al. (1992) and Duynkerke (1991) have clearly shown that the land cover strongly influences the fog formation by controlling fluxes at the ground. Over the past years, several experiments have been carried out to assess the realism of land surface parameterizations [e.g., Hydrological Atmospheric Pilot Experiment—Modélisation du Bilan Hydrique (HAPEX-MOBILHY); André et al. 1986] and soil–vegetation–atmosphere transfer schemes have greatly improved. In this study, the Interaction Sol Biosphère Atmosphère (ISBA; Boone et al. 1999, 2000; developed by Météo-France/CNRM) scheme is coupled to the atmospheric COBEL model. This allows the coupled COBEL–ISBA model to describe the interaction between the atmosphere, the surface, and the vegetation.

The objective of the work presented here is to develop a prediction system based on the use of the high-resolution coupled COBEL–ISBA model to perform short-term local forecasts of the structure of the atmospheric boundary layer at Paris-CDG. Although the coupled COBEL–ISBA numerical model can accurately simulate the evolution of the boundary layer, it is believed that further improvements in the forecast of local conditions, including low ceiling and/or poor visibility, may be accomplished by combining observations and 1D numerical modeling in an integrated forecast approach. As such the CNRM is currently engaged in a fog field experiment in which the following additional equipments have been operating at Paris-CDG since December 2002:

- a 30-m meteorological tower collecting observations of temperature and humidity in the surface boundary layer (levels of measurement: 1, 5, 10, and 30 m);
- the downward shortwave and longwave radiation fluxes are measured at the ground and on the roof of the airport terminal (about 45 m); in addition, the upward radiation fluxes are measured at the ground;
- soil temperature is measured at five levels between the ground and 1 m in depth (–5, –10, –20, –50, and –100 cm). As regards soil moisture measurements, some technical problems have prevented a proper working of these sensors during the studied winter season. For the forthcoming winter seasons, soil moisture observations are available in the ground, at –10, –20, –30, and –40 cm.

Added to this specific instrumentation, classical meteorological measurements are available, including 2-m temperature and humidity, visibility, ceiling, and precipitation.

The 1D model used in this study is presented in section 2. The assimilation procedure that attempts to optimally combine all the available information in clear-sky or cloudy conditions, is presented in section 3. And finally, the performance of the integrated forecast approach, the influence of the initial conditions, and the influence of the mesoscale flow (horizontal and vertical) are discussed in sections 4, 5, and 6, respectively.

2. Numerical model

Application of a 1D model for fog simulations provides many insights into fog physics, despite the poor estimation of horizontal heterogeneities. For local fog forecasts, the current 3D mesoscale models are too simple in terms of physical parameterizations (e.g., radiation or turbulence in a stable case) and resolution (e.g., vertical resolution). Thus, it is highly beneficial for the fog forecasting to precisely represent the radiative, microphysical, and turbulent processes within the boundary layer with as high a vertical resolution as possible. The atmospheric model used in this study is the high-resolution 1D COBEL model. A detailed description of the model can be found in Bergot (1993), Bergot and Guedalia (1994), and online (<http://www.rap.ucar.edu/staff/tardif/COBEL>), so only a brief description will be given hereafter.

The model equations are classically derived from the Boussinesq hypothesis, under the assumption of horizontal homogeneity. However, spatial heterogeneities are treated as an external mesoscale forcing and are evaluated from the Météo-France operational Aire Limitée Adaptation Dynamique Développement International (ALADIN) NWP model (model grid box of about 10 km). These mesoscale forcings (horizontal advection of potential temperature, horizontal advection of water vapor mixing ratio, vertical velocity, geostrophic wind, and cloud cover), varying with time and height, are used to modify the thermodynamic evolution of the boundary layer (see the schematic description of the method in Fig. 1).

The COBEL model equations are solved on a high-resolution vertical grid: near the surface, in the region of significance for fog and low clouds (i.e., below 200 m), numerical computations are made on 20 vertical levels (the first level is at 50 cm). The time step used is of 10 s except for the case of longwave radiation calculations, which are performed every 15 min. The main characteristics of the physical package used in the COBEL model are described below and include a parameterization of boundary layer turbulent mixing, cloud diagnosis, and parameterizations of longwave and shortwave radiation transfer.

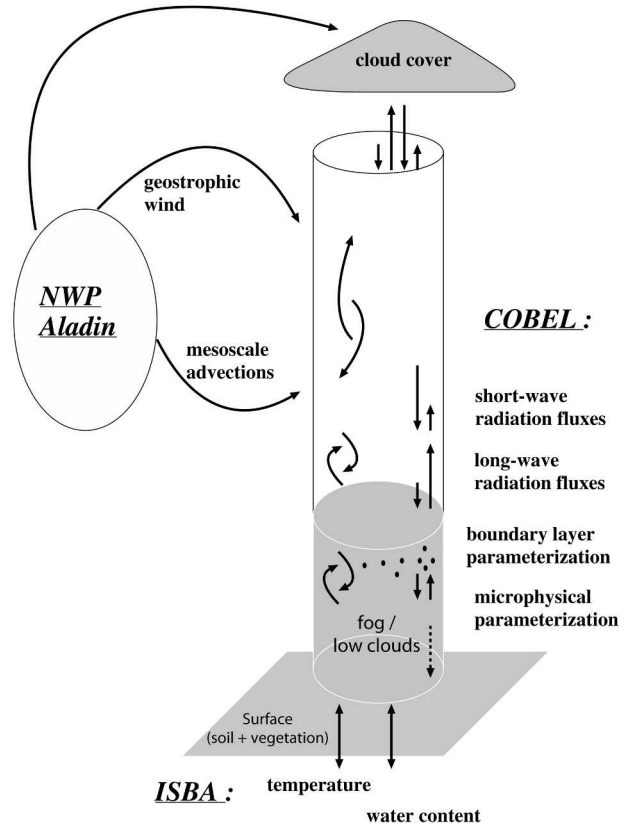


FIG. 1. Schematic depiction of the physical processes included in the COBEL-ISBA forecast method.

a. Summary of physical parameterization of the COBEL model

1) TURBULENCE SCHEME

A crucial model component for fog studies is the parameterization of turbulent vertical diffusion. The turbulent exchanges inside the boundary layer are treated using a 1.5-order turbulence closure scheme. The turbulent fluxes are parameterized using a predictive equation for the turbulent kinetic energy (TKE) and the mixing length is a function of the stability of the atmosphere. To simulate the formation and the evolution of a fog layer, it is of the utmost importance that the mixing length be especially adept at very stable stratification (thermal inversion before the appearance of fog) as well as unstable stratification (well-developed fog layer or during the dissipation phase). For stable stratification, the mixing length is a function of the Richardson number, according to Estournel and Guedalia (1987). For unstable stratification, the mixing length follows Bougeault and Lacarrere (1989).

Numerous comparisons with other models and simulations of real cases from field experiments have dem-

onstrated the quality of these turbulent parameterizations [see, e.g., Estournel (1988) for a detailed validation of the turbulence scheme under stable conditions, and Bougeault and Lacarrere (1989) or Bechtold (1992) for a detailed validation under unstable conditions].

2) MICROPHYSICS

The liquid water content, q_l , is computed as a prognostic variable, and the size distribution of the droplets is not considered:

$$\partial q_l / \partial t = -\overline{\partial w' q_l' p' / \partial z} \partial w' q_l' / \partial z + \partial G / \partial z + C. \quad (1)$$

Here, C represents the condensation term: as soon as humidity exceeds saturation, the excess is condensed assuming the conservation of energy and of the total water content (liquid and vapor). This implies that the entire grid box becomes saturated. Given the vertical resolution near the ground, where the fog and low clouds can appear, this parameterization seems accurate enough (Bergot 1993). The parameterization of the gravitational settling flux of droplets, G , is related to the liquid water content, q_l , by way of a settling velocity, v_i (Brown and Roach 1976):

$$G = v_i q_l. \quad (2)$$

A constant value of $v_i = 1.6 \text{ cm s}^{-1}$, derived from observations of fog droplet size distributions, is used in this study. Usually, mesoscale models do not include gravitational settling of clouds droplets. However, many studies (e.g., Brown and Roach 1976) have demonstrated that this process is crucial in simulating the fog layer.

Following Kunkel (1984), the visibility is deduced from the liquid water content:

$$\text{visibility(m)} = \frac{3.9}{144.7(\rho q_l)^{0.88}}. \quad (3)$$

3) RADIATION

The radiation exchanges are crucial for fog and low clouds formation, evolution, and dissipation, but the subject is too broad to be discussed here. As shown by numerous studies (e.g., André and Mahrt 1982 or Estournel 1988), the radiative cooling is frequently higher than the turbulent cooling or than mesoscale tendencies inside the nocturnal boundary layer. The COBEL model has an elaborate radiation scheme, which treats shortwave and longwave radiation separately.

The longwave radiation parameterization is a high-resolution spectral scheme that computes the longwave radiation fluxes at every model level for 232 spectral intervals between 4 and 100 μm (Vehil et al. 1989). The

radiative effect of the droplets is calculated inside the atmospheric window by relating linearly the longwave optical depth to the liquid water content.

The shortwave radiation is computed following the monospectral scheme of Fouquart and Bonnel (1980). The effect of cloud droplets is parameterized by computing the shortwave optical thickness, which is related to the liquid water content. The single-scattering albedo of fog and low cloud is related to the optical thickness.

b. The ISBA surface scheme

The ISBA surface scheme describes the interactions between the land surface and the overlying atmosphere (Noilhan and Planton 1989). The accuracy of the land surface scheme has a significant impact on the evolution of near-surface atmospheric variables, influencing the surface energy and moisture budget. The COBEL model is coupled with the multilayer surface-vegetation-atmosphere transfer scheme ISBA-DF (Boone 1999, 2000). In this study, seven soil layers are used to represent a soil column of 2-m depth. The assumption that the vertical temperature or water content gradients are largest near the surface suggests that the grid spacing must be smaller there. The three grid levels closest to the surface are used to resolve the penetration depth of the diurnal temperature (the thickness of the first soil layer is 0.5 cm and that of the second soil layer is 2.5 cm).

The main advantage of the ISBA parameterization is that it is capable of accurately reproducing the energy and water budgets with a simple set of equations as confirmed by the Project for Intercomparison of Land-Surface Parameterization Schemes (PILPS; Henderson-Sellers et al. 1995; Chen et al. 1997) or Calvet et al. (1999).

3. Estimation of the initial state

The challenge of low ceiling and/or poor visibility forecasting begins with the difficulty of accurately representing the initial state of the atmosphere and of the soil. For example, Pagowski et al. (2004) noted that the initialization of soil moisture is important, and even differences of 10% between the measured and estimated soil water content could lead to large errors in fog forecasting.

The central problem in developing a model for fog and low clouds is the assimilation of local observations. The goal of the assimilation system associated with COBEL-ISBA is to produce a physically consistent representation of the atmospheric and soil profiles. Our

basic idea is to try to optimize the use of all available local observations. This information can be summarized by observations from field experiments, vertical profiles coming from a previous COBEL–ISBA forecast, and operational forecasts from the 3D ALADIN NWP model. But the assimilation procedure associated with COBEL–ISBA can do more than simply optimally interpolate observations; it also reconstructs profiles from observations that are related in a complex way to the variables to be analyzed (e.g., the assimilation procedure under cloudy conditions or the assimilation procedure for soil profiles). In fact, the observations used are not only composed by direct—or closely related—measurements of the model state variables, like temperature and humidity, but also by indirect observations, like radiation measurements, which contain useful information about the atmospheric initial conditions. The assimilation procedures used to construct the initial conditions are as follows:

- estimate the atmospheric vertical profile of temperature and humidity in a one-dimensional variational data assimilation (1DVAR) framework;
- if low clouds or fog are detected, adjust the atmospheric profiles to introduce the cloud cover;
- estimate the vertical profiles of temperature and water content within the soil.

a. Assimilation of atmospheric profiles: 1DVAR

The estimation of the temperature and humidity initial profiles uses a variational assimilation approach. The variational approach to the assimilation of data into NWP models has been described in a number of articles (e.g., Le Dimet and Talagrand 1986). The principle is to minimize a penalty or cost function $J(x)$, with respect to a control variable x containing the description of the atmospheric state to be analyzed. This function $J(x)$ measures the degree of fit to the observations and to some a priori information (background), and takes the form

$$J(x) = \frac{1}{2}(x - x_b)^T \mathbf{B}^{-1}(x - x_b) + \frac{1}{2}[\mathbf{y} - \mathbf{H}(x)]^T \mathbf{R}^{-1}[\mathbf{y} - \mathbf{H}(x)], \quad (4)$$

where x_b is the background state (a previous short-range COBEL–ISBA forecast), \mathbf{B} is its expected error covariance matrix, \mathbf{y} is the observation vector, \mathbf{H} is the observation operator (projection from model space to observation space), and \mathbf{R} is the error covariance matrix of the observations.

The minimum of $J(x)$ imposed by $\nabla_x J = 0$ gives the analysis state x_a :

$$x_a = x_b + \mathbf{B}\mathbf{H}^T(\mathbf{H}\mathbf{B}\mathbf{H}^T + \mathbf{R})^{-1}[\mathbf{y} - \mathbf{H}(x_b)]. \quad (5)$$

This analysis method is applied to our 1D vertical problem and is consequently called 1DVAR.

The observed state \mathbf{y} contains the 2-m observations as well as measurements issued from the tower. Observational errors are assumed to be uncorrelated (\mathbf{R} is a diagonal matrix), and their variance is set to $(0.1 \text{ K})^2$ for temperature and to $(0.1 \text{ g kg}^{-1})^2$ for humidity (coming from the accuracy of the measurements). The vertical profiles from the 3D ALADIN NWP model are also added to the vector \mathbf{y} . The correlation function for these data has the form $(1 + dz/do) \exp(-dz/do)$, where dz is the vertical distance and do the distance of correlation. The variance is set to $(2 \text{ K})^2$ for temperature and $(0.5 \text{ g kg}^{-1})^2$ for humidity. These values are found after a comparison between ALADIN and the observations. The observation operator \mathbf{H} simply consists of a linear interpolation.

The variational analysis requires an estimation of the background error statistics (\mathbf{B} matrix). Different methods can be used to estimate the model errors statistics [like the Monte Carlo method, or the so-called National Meteorological Center (NMC, now known as the National Centers for Environmental Prediction) method]. However, applying these methods would require one to run simulations over at least a whole winter season. In our case, it was not possible to apply these methods for deriving \mathbf{B} . This is planned in future work, once the feasibility of this integrated forecast method has been demonstrated. In a first stage, we have imposed the correlation function to take the form of $(1 + dz/dg) \exp(-dz/dg)$, and the variances vary linearly from the surface to the top of the model, namely from $(0.5 \text{ K})^2$ to $(2 \text{ K})^2$ for temperature and from $(0.2 \text{ g kg}^{-1})^2$ to $(0.5 \text{ g kg}^{-1})^2$ for humidity. These error statistics are imposed arbitrarily but allow the initial profile to be very close to the observations near the surface, and to get close to the 3D NWP forecast above the boundary layer. The impact of the error statistics on the fog and low cloud forecast will be studied in future work.

Concerning the initialization of the wind profile, the 10-m wind is the only available measurement. As is often the case for boundary layer simulations, the profile of geostrophic wind from the NWP model is used to reconstruct the wind profile [following the classical boundary layer profile; see Stull (1988)]. This method has been successfully used in previous studies [for more detail see Bergot (1993), Guedalia and Bergot (1994), or Roquelaure (2004)]. A comparison of the 10-m

wind intensity between COBEL-ISBA and observations shows that the errors in the initial conditions of COBEL-ISBA 10-m wind intensity are of the same order of magnitude as the accuracy of the measurement (the bias is equal to 0.4 m s^{-1}). Moreover, no major spinup problem was found for the wind intensity.

b. Assimilation of fog layer

The following procedure is used to modify the initial profile of temperature and humidity when fog is detected. The main goal is to accurately represent the atmospheric boundary layer structure inside the fog layer. To precisely simulate the evolution of fog, and particularly to accurately forecast the dissipation phase of fog, it is important to accurately initialize the fog layer characteristics. The major problem is in estimating the fog depth, and in adjusting the atmospheric profiles inside the fog layer in order to represent the dynamics as accurately as possible.

It is now well known that mature fog events consist of well-mixed atmospheric layers as a consequence of the profile of radiative divergence. Consequently, the atmospheric profiles inside the fog layer are adjusted following the hypothesis that total water content (liquid and vapor) is constant, that the temperature follows a moist-adiabatic profile, and that the atmosphere is saturated. Above the fog layer, the atmospheric profiles issued from the 1DVAR scheme are not modified.

The fog depth is determined using an iterative method with the goal of minimizing the model error on radiation flux divergence. Atmospheric profiles are constructed following the previous method, and the COBEL radiation scheme is used to compute the radiation fluxes for various fog depths. An example of the variation of the error on the longwave radiation fluxes as a function of the estimated fog depth is presented in Fig. 2a. This error behaves typically, with rapid variation for estimated fog top just above the level of measurement. This behavior implies that fog depth determined by minimizing the error on the longwave radiation flux at one level is very sensitive to measurement errors (typical accuracy of the order of a few W m^{-2}) or to mesoscale model errors (poorly forecast upper-level clouds).

To simulate the evolution of radiation fog, it is important that the radiation flux divergence is correctly forecast. Therefore, the method used to estimate the fog depth is to minimize the error on the radiation fluxes divergence between the two levels of measurement (the ground and about 45 m). An example of the variation of the error of the radiation divergence as a function of the estimated fog depth is shown in Fig. 2b for the case previously presented. This error has a clear

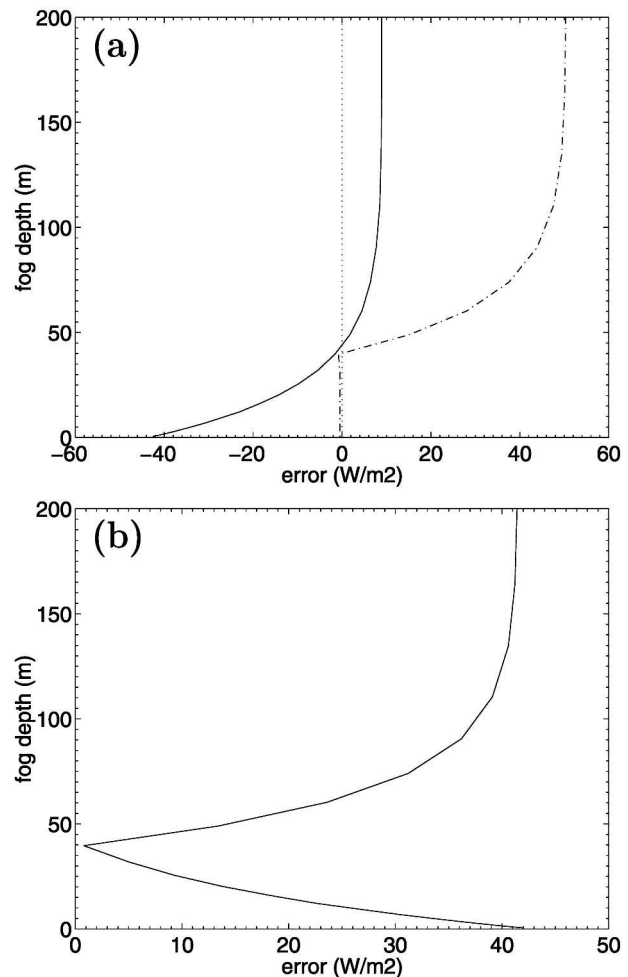


FIG. 2. Fog case of 28 Dec 2002 at 0300 UTC. (a) Error on the simulated longwave radiation fluxes at ground level (solid line) and at the top of the airport terminal (dashed line) as a function of fog depth. (b) Error on the vertical divergence (between the ground and the top of the airport terminal) of the longwave radiation fluxes.

minimum for a given fog depth (this behavior is typical). Consequently, it is absolutely essential to have at least two accurate longwave radiation flux measurements at different levels to properly estimate the fog depth.

If the fog layer is broadly above the upper level of measurement (about 25% of cases for the studied winter season), the vertical gradient between the two levels of measurements is about zero, and the methodology previously presented will not be applicable. In this case, the fog depth is determined by minimizing the error on the shortwave radiation at the ground during the day (see the following section on the initialization of low clouds for a detailed explanation), or by minimizing the error on longwave radiation at the ground during the night.

The assimilation procedure has been performed every 3 h, from 1 December 2002 to 30 April 2003. Figure 3 shows a scatterplot between the simulated downward radiation fluxes and the observed fluxes when fog is detected. During the 2002/03 winter season, the assimilation of fog has been activated 23 times. Without the assimilation of the fog layer (Fig. 3a), radiation fluxes have a significant bias of -45.8 W m^{-2} at the initial time. After the assimilation, the bias is of the same order of magnitude as the accuracy of the measurement (Fig. 3b).

c. Assimilation of low clouds

When low clouds are detected by ceilometers, the initial profiles of temperature and humidity are modi-

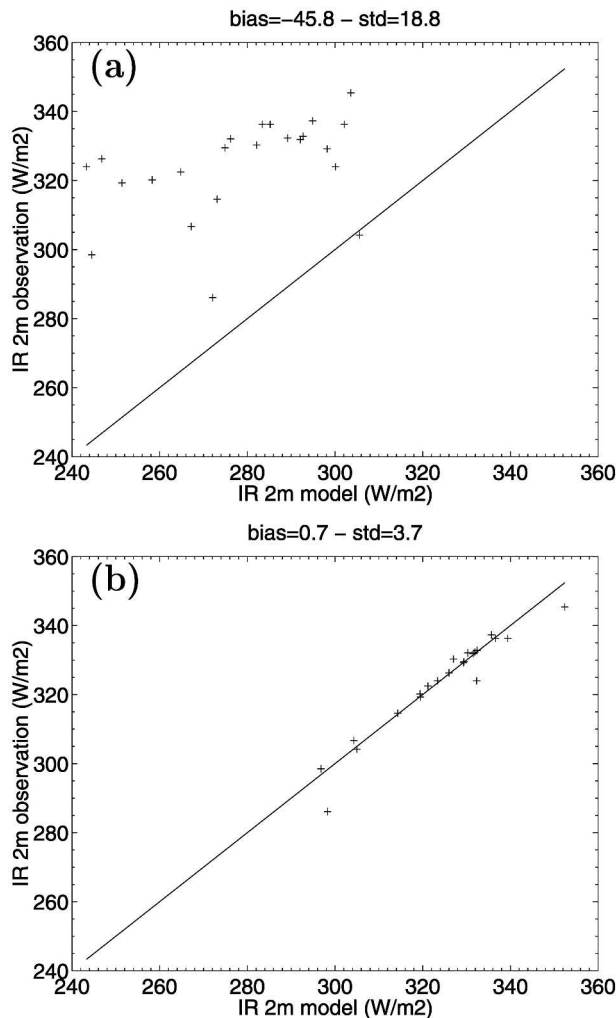


FIG. 3. Scatterplot comparing the observed and modeled downward longwave radiation fluxes at the ground for the initial condition in cases of fog. (a) Initial conditions issued from the 1DVAR; (b) initial conditions issued from the procedure of fog initialization.

fied below and inside the cloud layer. The cloud base is determined from ceilometer measurements, and the main problem is then to estimate the cloud top and the atmospheric profiles inside and below the cloud.

The initial profiles are determined as follows:

- Below the cloud layer—The atmospheric profile of temperature is modified according to the temperature at the ground under the hypothesis of a dry-adiabatic profile. The humidity is assumed to be at saturation value at cloud base, and the profile of humidity is interpolated linearly between this level and the ground.
- Inside the cloud layer—The temperature is determined from the temperature at cloud base under the hypothesis of a moist-adiabatic vertical gradient. The humidity is assumed to be saturated, and the liquid water content is estimated assuming that the total water content (liquid and vapor) is constant.
- Above the cloud layer—The profiles issued from the 1DVAR scheme are not modified.

The cloud-top height is determined using an iterative method. Atmospheric profiles are constructed following the previous method, and the COBEL radiation scheme is used to compute the radiation fluxes for various cloud tops. An example is given in Fig. 4 for the low-cloud case of 2 February 2003 at 1200 UTC. This figure shows that the error on shortwave radiative fluxes exhibits a clear minimum for a given cloud-top height. This behavior is always observed and the cloud vertical extent can therefore be estimated during the day. One also can see that the estimation of cloud top

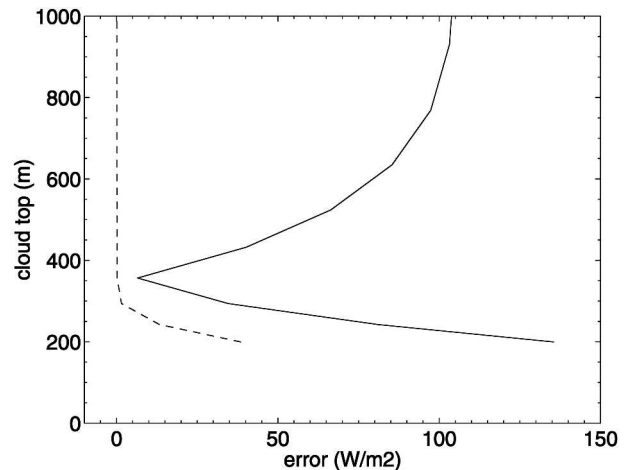


FIG. 4. Low cloud case of 2 Feb 2003 at 1200 UTC. Error on the simulated radiation fluxes at the ground as a function of cloud-top height. Shortwave: solid line. Longwave: dashed line.

is not very sensitive to errors in measured shortwave radiative fluxes or errors in mesoscale upper-level clouds. In contrast, the error in the longwave radiative fluxes exhibits no clear minimum as a function of the estimated cloud top. Consequently, it is very difficult to accurately estimate the cloud top during the night. However, the error in the estimated cloud-top height does not have a significant effect on the longwave radiative fluxes and thus on the radiative cooling during the night. But an error on the cloud height has a much more pronounced effect during the day because of the strong effect on the shortwave radiation.

During the 2002/03 winter season (from 1 December 2002 to 30 April 2003), the assimilation procedure of low clouds has been activated for about a third of the cases. As was previously done for the fog cases, the simulated downward radiation fluxes have been compared to the observed ones when low clouds are assimilated. The procedure of low cloud initialization clearly reduces the bias on radiation fluxes (from -41.9 to -1 W m^{-2} for the downward longwave radiation fluxes at the ground; Fig. 5).

d. Assimilation of soil profiles

The initialization of land surface prognostic variables is crucial in short-range weather forecasting. Because soil moisture and temperature link the energy budget at the surface by regulating heat fluxes, accurate estimates of soil moisture and temperature are of the utmost importance for the study of boundary layer processes and, consequently, for fog and ceiling forecasts. Unfortunately, direct observations of soil moisture were not available during the winter season studied, and it was necessary to estimate indirectly the soil profiles in balance with the atmospheric state by using the ISBA model and atmospheric measurements. Detailed description of the soil assimilation methodology used in this study can be found in Habets et al. (1999) or Calvet et al. (1999). These previous studies have also demonstrated that this assimilation procedure allows for the estimation of the soil state in a realistic way. However, the subject is too broad to be discussed here and only a brief description of the soil assimilation procedure will be given hereafter.

To keep consistency inside the soil, the same assimilation method is used to estimate both the temperature and moisture profiles. The soil profiles at the initial time are estimated from a guess field (the soil profiles from the previous ISBA simulation), by integrating the ISBA model during the assimilation window. The ISBA model is driven by measured atmospheric fields—the 2-m temperature and humidity, the 10-m

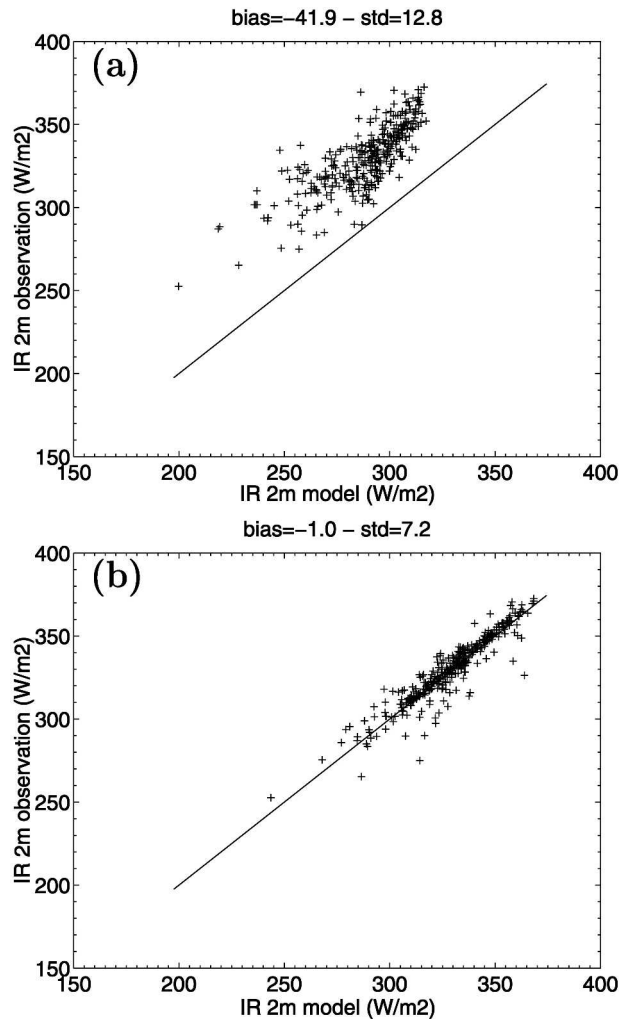


FIG. 5. Scatterplot comparing the observed and modeled downward longwave radiation fluxes at the ground level for the initial condition in cases of low clouds. (a) Initial conditions from 1DVAR; (b) initial conditions from the procedure of low cloud initialization.

wind, the surface radiation fluxes, and surface precipitation—during the assimilation window at a frequency of 15 min, and simulates the profiles inside the soil in balance with the observed atmospheric state. This assimilation procedure can be seen as a 2DVAR assimilation method.

A comparison between the estimation of the soil profile and the measurements inside the soil will be done during the forthcoming winter. Moreover, the initial conditions inside the soil have a significant impact on the evolution of near-surface atmospheric variables, and a comparison between the observed and simulated 2-m temperature will be performed in this study in order to validate this soil assimilation method (section 4).

4. Results

The COBEL–ISBA model has been run every 3 h, up to 21-h forecasts, starting from 0000, 0300, 0600, 0900, 1200, 1500, 1800, and 2100 UTC (local time = UTC + 1) during a 5-month period (from December 2002 to April 2003). The initial conditions are derived from the assimilation procedure previously described. As a first step, the mesoscale forcing (varying with time and height) only consists of the geostrophic wind and the cloud cover (the horizontal advections and vertical velocity are not taken into account, and their effects will be studied in section 6).

In a first stage, the forecasts of the LVP conditions at Paris-CDG are studied. The LVP conditions correspond to visibility lower than 600 m and/or ceiling lower than 200 ft (about 60 m). The LVP conditions are defined every 30 min: if these thresholds are exceeded at least once, the period is defined as LVP. The occurrence of observed and forecast LVP conditions are then compared for each 30-min time periods. In a second stage, the forecast of thermodynamical parameters is examined in order to better understand the reasons of the errors, and consequently to explore some way of improving them.

a. Verification of the LVP forecasts

The statistics produced to study the quality of the LVP forecasts are based on the hit ratio (HR), false alarm rate (FAR), frequency bias index (FBI), and critical success index (CSI). If a is the number of observed and forecast events, b the number of not observed and forecast events, and c the number of observed and not forecast events, these scores are defined by

$$\begin{aligned}
 \text{HR} &= \frac{a}{a + c}, \\
 \text{FAR} &= \frac{b}{a + b}, \\
 \text{FBI} &= \frac{a + b}{a + c}, \\
 \text{CSI} &= \frac{a}{a + b + c}.
 \end{aligned}
 \tag{6}$$

Figure 6 shows that HR is larger than FAR until a forecast time of about +4 h. Between +4 and +9 h, HR and FAR are of the same magnitude (between 0.5 and 0.6). Afterward, FAR becomes larger than HR, and the COBEL–ISBA forecast seems no more useful. The HR is plotted against FAR, in a so-called relative operating

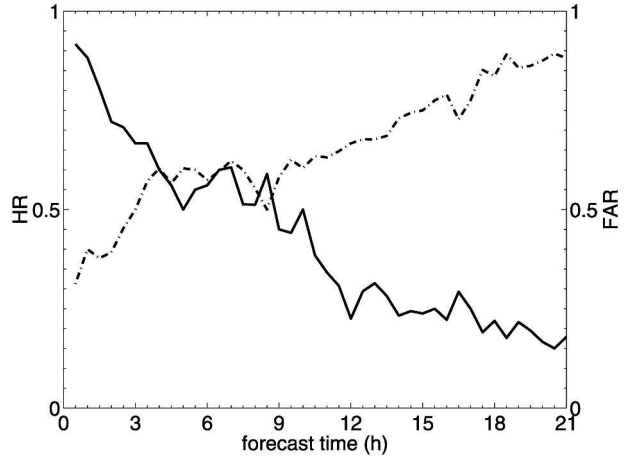


FIG. 6. Comparison of the observed and forecasted LVP conditions for the 2002/03 winter. Hit ratio (HR): solid line. False alarm rate (FAR): dashed line.

characteristic (ROC) diagram in Fig. 7. One can see in this figure that the COBEL–ISBA LVP forecasts have a small bias for short-term forecasts, which indicates that the forecasting system has a small tendency to overpredict LVP conditions. However, a comparison with the man-made operational forecasts (Fig. 7) illustrates the fact that the COBEL–ISBA forecast could be

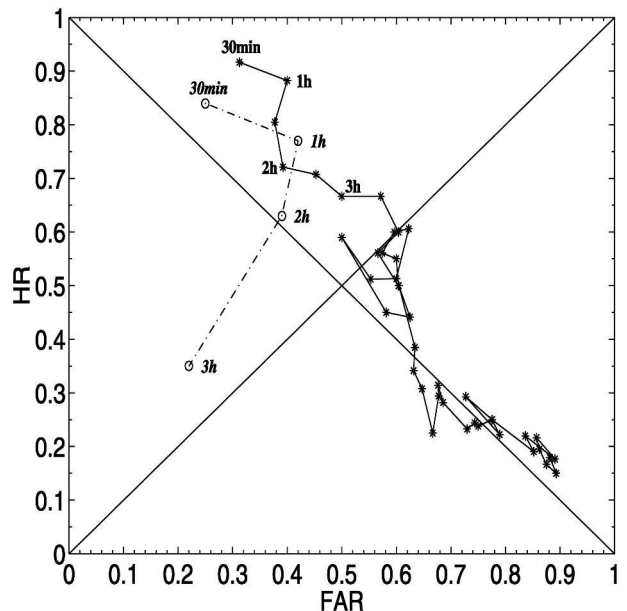


FIG. 7. Comparison of the observed and forecasted LVP conditions for the 2002/03 winter, in an ROC curve format. Solid line and *: forecast from the COBEL–ISBA model every 30 min, from 30 min to 21 h; dashed line and o: operational LVP forecast at 6 h for a forecast time of 30 min, 1 h, 2 h, and 3 h.

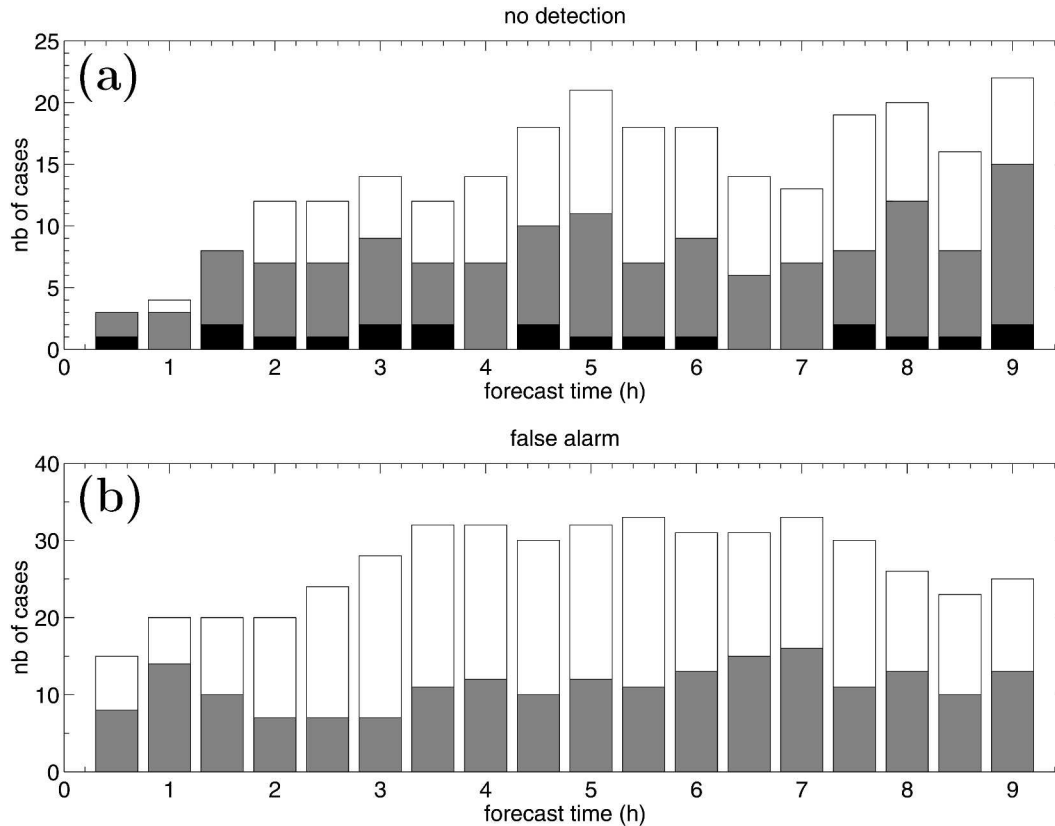


FIG. 8. Distribution of the error cases for (a) no-detection and (b) false alarm. Black: error in visibility only; gray: error in ceiling only; and white: error in both visibility and ceiling.

helpful to forecasters in predicting LVP conditions even at a very short range.

The distribution of the LVP forecast errors into errors in visibility, errors in ceiling, or both, is plotted in Fig. 8. Concerning the misses, the number of errors in visibility only is relatively small (one case). This result shows that fog events are fairly well forecast by the COBEL-ISBA model. In opposition, Fig. 8 shows that about one-half of the forecast errors in LVP conditions are due to an error in the forecast of low clouds (error on ceiling only). This result could be a consequence of the missing mesoscale advections, which are important for performing a correct forecast of low clouds (e.g., Driedonks and Duynkerke 1989). This point will be studied in section 6. With regard to the false alarm rate, Fig. 8b shows that only visibility is unaffected by this statistic. This is due to the fact that low ceiling is systematically forecast when fog is present. The main conclusion of this discussion is that the majority of errors occur when low cloud is forecast.

To examine the dependence of forecast skill as a function of the initialization time, and particularly between day and night, the critical success index (CSI) has

been calculated for different initialization times (Table 1). CSI is a widely used performance measure of rare events, but is very sensitive to the number of events as shown in Table 1 where CSI rapidly varies during the day (the number of events is smaller during the day). Consequently, the number of cases is too small to statistically evaluate the quality of the LVP forecasts for the various initialization times. However, if all forecasts are considered (disregarding the initialization time), it appears that the LVP forecast is of good quality during the first 3–4 h. This result will be explored in more detail during the forthcoming winters.

b. Quality of the thermodynamical parameters forecast

After evaluating the quality of LVP forecasts, the quality of the thermodynamical parameters forecast is analyzed. For continuous parameters such as temperature, one uses the bias (B), the root-mean-square error (rmse), and the reduction of variance (RV) to assess the quality of the forecast. The bias or mean error is given by

TABLE 1. CSI of COBEL–ISBA LVP predictions for different beginning times of +30 min, +1 h, +2 h, +3 h, +4 h, +5 h, and +6 h forecasts.

	0000 UTC	0300 UTC	0600 UTC	0900 UTC	1200 UTC	1500 UTC	1800 UTC	2100 UTC	All
30 min	0.80	0.60	0.78	0.33	1.00	0.40	0.71	0.67	0.65
1 h	0.40	0.55	0.60	0.40	1.00	0.50	0.63	0.50	0.56
2 h	0.56	0.64	0.46	0.33	0.00	0.75	0.63	0.43	0.49
3 h	0.29	0.54	0.36	0.33	0.00	0.67	0.38	0.50	0.40
4 h	0.27	0.31	0.33	0.25	0.25	0.43	0.38	0.29	0.31
5 h	0.31	0.24	0.25	0.00	0.50	0.25	0.29	0.44	0.28
6 h	0.38	0.25	0.38	0.00	0.33	0.33	0.33	0.33	0.32

$$B = \frac{1}{n} \sum_{i=1}^n (f_i - o_i), \quad (7)$$

where f_i is the forecasted value and o_i the observed value.

The rmse is given by

$$\text{rmse} = \sqrt{\frac{1}{n} \sum_{i=1}^n (f_i - o_i)^2}. \quad (8)$$

The RV is a skill score depending on the observed climatology and is given by

$$\text{RV} = 1 - \frac{\sum_{i=1}^n (f_i - o_i)^2}{\sum_{i=1}^n (o_i - \bar{o})^2}, \quad (9)$$

where \bar{o} is the mean observation.

In order for these results to be comparable with other studies of the quality of NWP forecast products, the quality of the 2-m parameters is specially considered. Given the poor accuracy of the humidity measurement close to saturated conditions, we have chosen to focus our attention on the 2-m temperature. Figure 9 shows that the quality of the 2-m temperature prediction by the COBEL–ISBA system is superior to current model output statistics (MOS) systems up to +3 h, and is of the same order of magnitude up to +6 h (see Wilson and Vallee 2003). To see the effect of the starting time on the quality of the temperature prediction, Table 2 displays the RV for a +3 h forecast and for the different beginning times. This table demonstrates that the quality of the COBEL–ISBA forecast is better during the night and that the nocturnal inversion is also well predicted (small variation of the RV in the vertical). During the day, the skill scores are worse at all levels, and the 1D forecast seems more helpful during the night.

Figure 10 illustrates that the temperature prediction

is unbiased when considering all forecasts starting every 3 h (the bias is of the same order of magnitude as the accuracy of the measurements). However, the spread grows quickly during the first hours of simulation: the rmse increases from 0.4°C at the initial time to 0.9°C at +1 h, 1.2°C at +2 h, and 1.4°C at +3 h. This point needs to be studied in detail to improve the short-term forecast of the COBEL–ISBA model. Figure 10a illustrates also that the initial conditions are close to the observations and that the assimilation scheme works well.

Figure 11 shows that the 10-m wind intensity is well initialized and well forecast during the first hours of simulation, without major spinup problems.

To examine the quality of the radiative parameters, the scatterplot of the longwave radiation fluxes at 45 m is plotted Fig. 12. Some problems always exist in the mesoscale clouds, despite the initialization of the low-level clouds. In particular, a bias of about -10 W m^{-2} already exists at the initial time and remains almost constant during the forecast. These scatterplots clearly illustrate that clouds are not well predicted by the

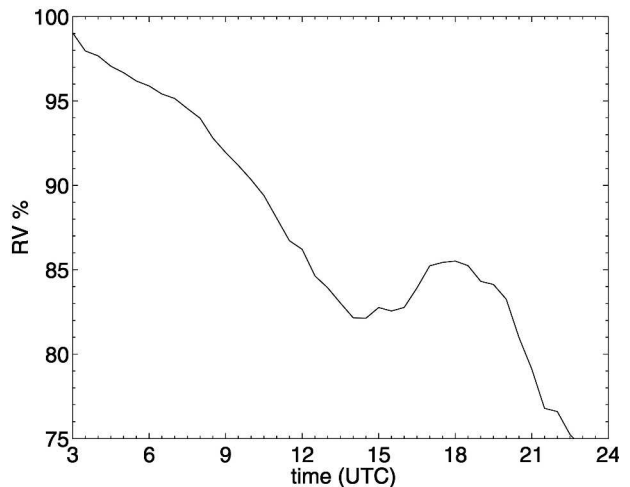


FIG. 9. Percent reduction of variance (RV) for the temperature at 2 m, for the simulations beginning at 0300 UTC.

TABLE 2. The RV for the atmospheric temperature at 1, 2, 5, 10, and 30 m, as a function of the starting time, for a +3 h forecast.

	0000 UTC	0300 UTC	0600 UTC	0900 UTC	1200 UTC	1500 UTC	1800 UTC	2100 UTC
T 1 m	0.96	0.96	0.91	0.90	0.93	0.98	0.95	0.95
T 2 m	0.95	0.96	0.93	0.92	0.94	0.98	0.95	0.95
T 5 m	0.97	0.96	0.92	0.91	0.94	0.98	0.96	0.96
T 10 m	0.97	0.96	0.93	0.90	0.89	0.97	0.97	0.96
T 30 m	0.97	0.96	0.93	0.90	0.88	0.97	0.96	0.97

ALADIN NWP model. Additional analysis of this point is needed in order to improve the forecast of the thermodynamical parameters and, consequently, the forecast of the LVP conditions.

c. Example of fog simulation

To illustrate the previous results, a typical radiation fog event that took place during the night of 3 March 2003 is studied in detail. The fog layer appears around 0300 UTC at the ground. The vertical development reaches the top of the airport terminal (about 45 m)

around 0700 UTC, and the LVP conditions ceased around 0900 UTC. During the night, the wind is weak ($1\text{--}2\text{ m s}^{-1}$), and a thermal inversion of about 4°C between 1 and 30 m was observed before the onset of the fog.

Figure 13 shows the results of a forecast beginning at 0000 UTC. The onset of fog is well forecast (Fig. 13a). However, the evolution of the fog layer thickness is underestimated (Fig. 13c). The major consequence is that the drying of the atmosphere happens a bit too quickly (Fig. 13b), and the end of the LVP conditions is forecast 30 min too soon (for a forecast time of

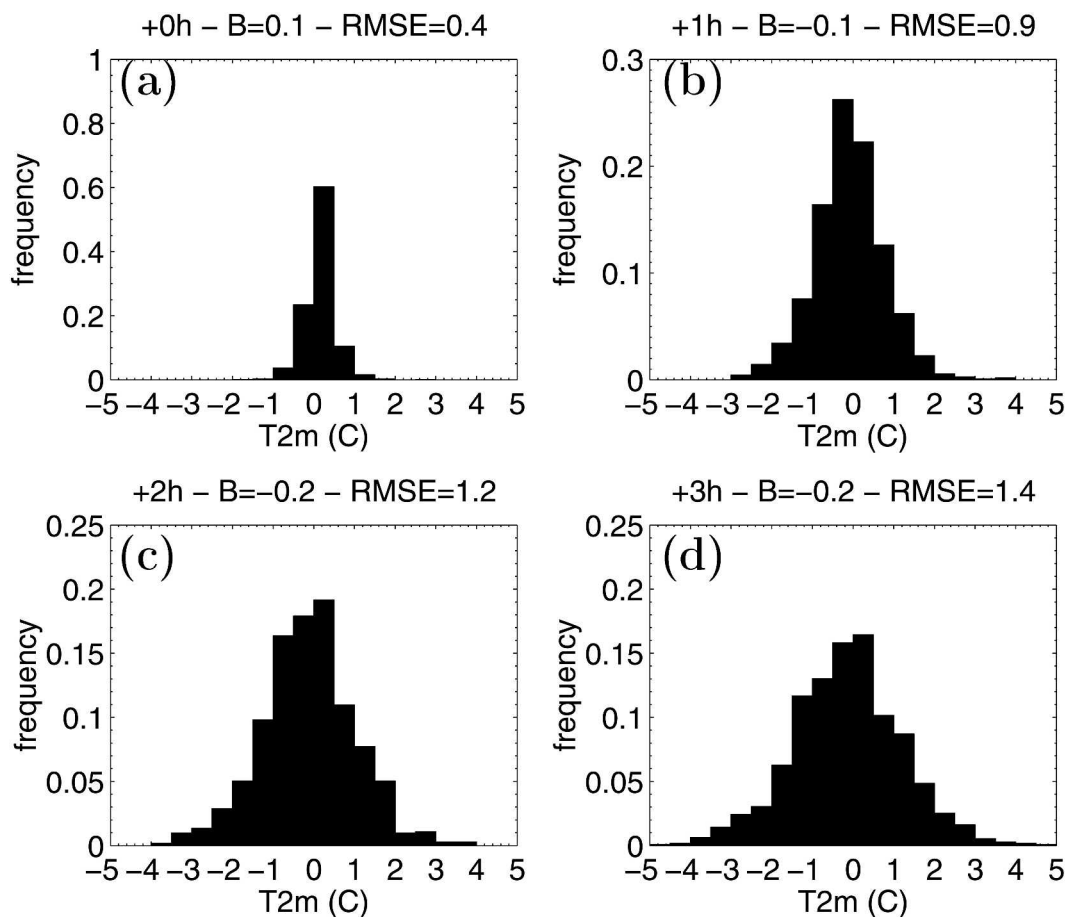


FIG. 10. Distribution of the error on the temperature at 2 m ($^\circ\text{C}$) for the (a) initial conditions, (b) +1 h forecast, (c) +2 h forecast, and (d) +3 h forecast.

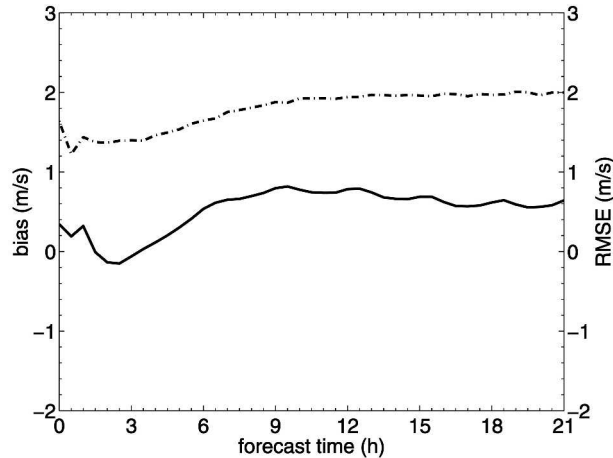


FIG. 11. Bias (solid line) and rmse (dashed line) for the intensity of the 10-m wind in function of the forecast time.

+9 h). The thermal profile is quite well forecast (not shown).

Figure 14 shows the results of a forecast beginning at 0600 UTC, after the onset of the fog layer. The initialization of the fog layer is quite accurate (well-forecast radiation fluxes and boundary layer profiles; not shown) and leads to a quite well-forecast evolution of the horizontal visibility (Fig. 14a) and of the relative humidity (Fig. 14b). In opposition to the previous forecast, the fog layer now reaches the top of the airport terminal, as was observed (Fig. 14c). The thermodynamical structure of the boundary layer is well forecast with an inversion above the fog layer, as shown by the humidity isocontours (Fig. 14d).

This example of a radiation fog event allows us to illustrate in one case that the assimilation procedures work well with or without fog and that the COBEL-ISBA model is able to describe the physical processes occurring in the radiation fog. However, in order to make successful fog forecasts, it is of the utmost impor-

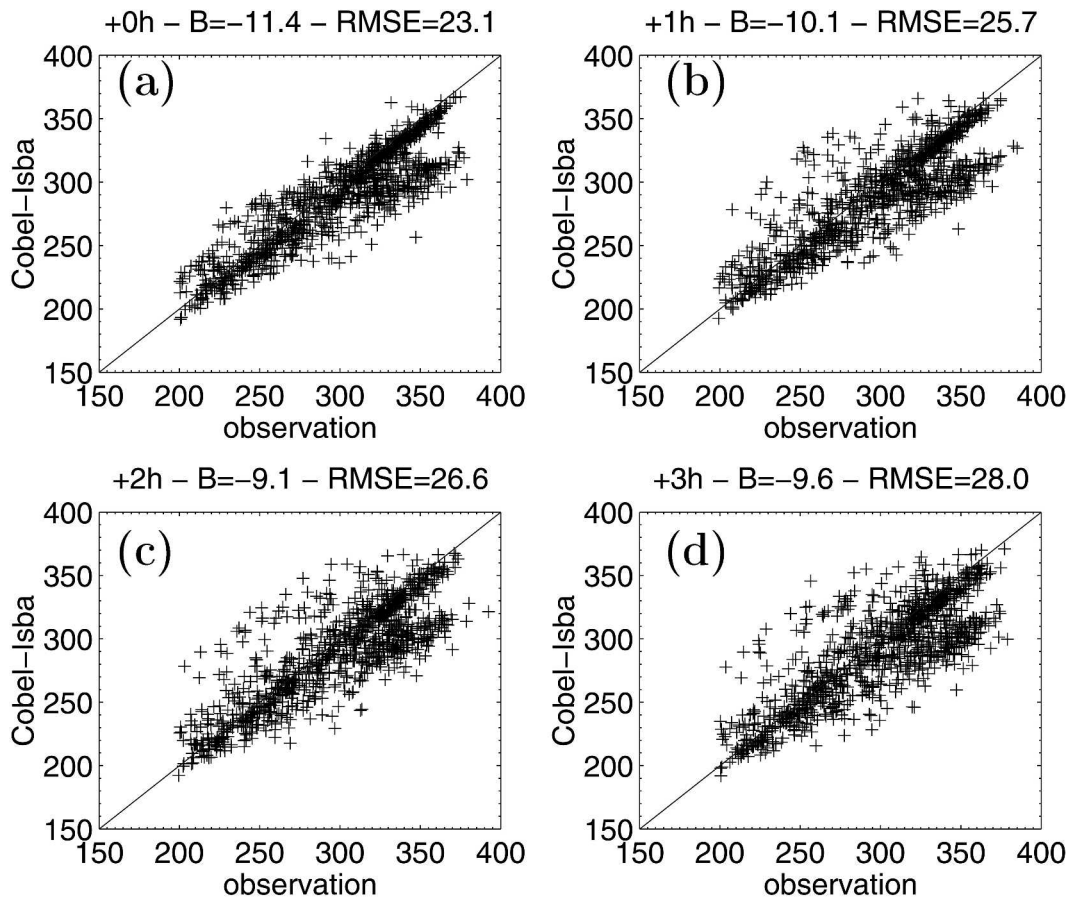


FIG. 12. Scatterplot comparing the observed downward infrared radiative fluxes (W m^{-2}) at 45 m with the calculated value from the 1D COBEL-ISBA model, in the (a) initial conditions, (b) +1 h forecast, (c) +2 h forecast, and (d) +3 h forecast.

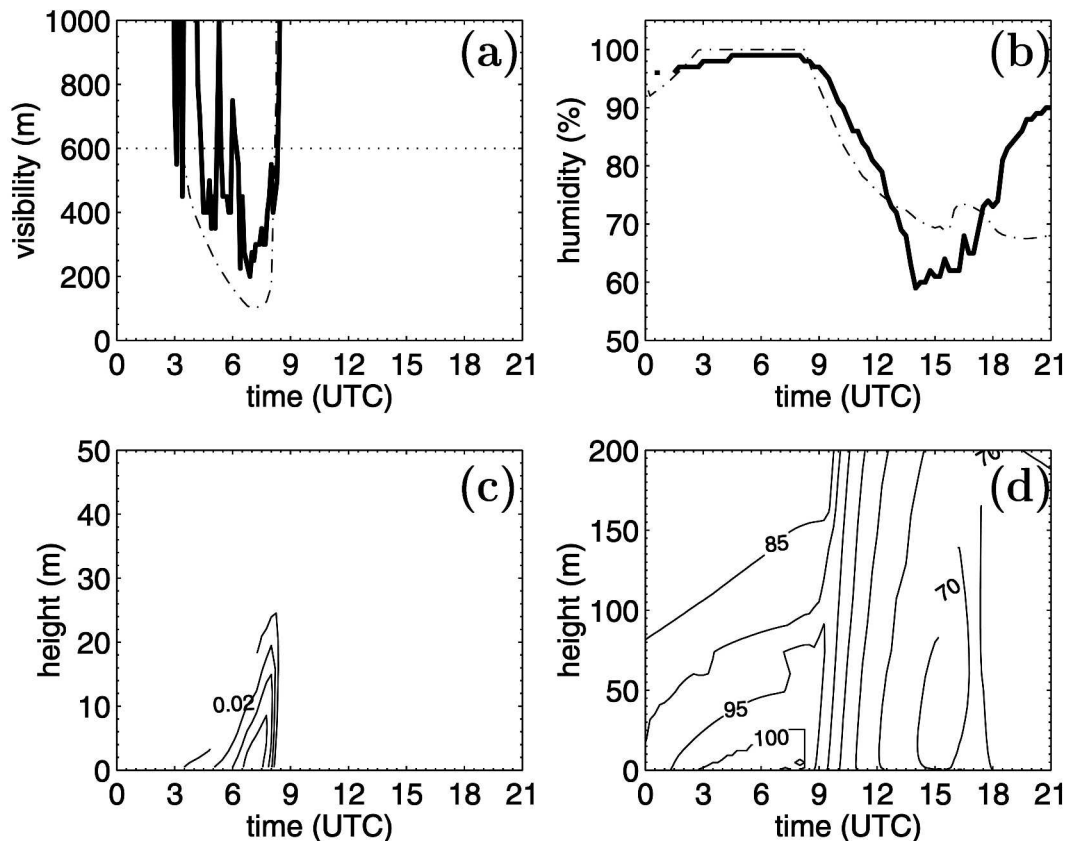


FIG. 13. Case of 3 Mar 2003 at 0000 UTC. (a) Horizontal visibility at 2 m and (b) humidity at 1 m. Bold line: observation; dashed line: COBEL-ISBA simulation. (c) Contour of liquid water content: the contour interval is 0.02 g kg^{-1} . (d) Contour of relative humidity: the contour interval is 5%.

tance to have a good knowledge of the initial conditions. This point is studied in the next section.

5. Influence of initial conditions

The previous results do not depend solely on the inclusion of observations (associated with the local assimilation scheme) but also on the higher vertical resolution and on the detailed physical parameterizations of the COBEL-ISBA model. For this reason, another set of forecasts has been performed where the 1D simulations are initialized from the operational ALADIN NWP model, without running the local assimilation scheme (the atmospheric and soil ALADIN parameters are simply linearly interpolated onto the COBEL-ISBA grid). This allows us to demonstrate the effect of local observations on the forecast skill. As previously, the mesoscale forcing only consists of the geostrophic wind and the cloud cover.

a. Quality of the LVP forecast

The ROC diagram for forecasts performed without the local assimilation scheme is plotted Fig. 15 (cf. with

Fig. 7 for the COBEL-ISBA forecasts with the local assimilation scheme). This figure shows that the simulation without the assimilation scheme produces a good HR: 97% for a +1 h forecast, 93% for +2 h forecast, and 90% for +3 h forecast. Unfortunately, the FAR has about the same magnitude as the HR: 93% for a +1 h forecast, 90% for a +2 h forecast, and 89% for a +3 h forecast. This result demonstrates that the COBEL-ISBA forecasts without assimilation have a significant bias. To illustrate this bias, FBI is given in Table 3. FBI has the same magnitude for the forecast based on persistence and for the COBEL-ISBA forecast with initial conditions issued from the assimilation scheme. On the other hand, the COBEL-ISBA forecasts issued with ALADIN's initial conditions show a very strong FBI at the initial time (15 for a +30 min forecast), and the FBI decreases slowly thereafter (6.5 for a +6 h forecast). This illustrates that the bias is a consequence of erroneous initial conditions.

To go further in the comparison between the various forecasts, the evolution of HR (Fig. 16a) and the evolution of FAR (Fig. 16b) are plotted as a function of the

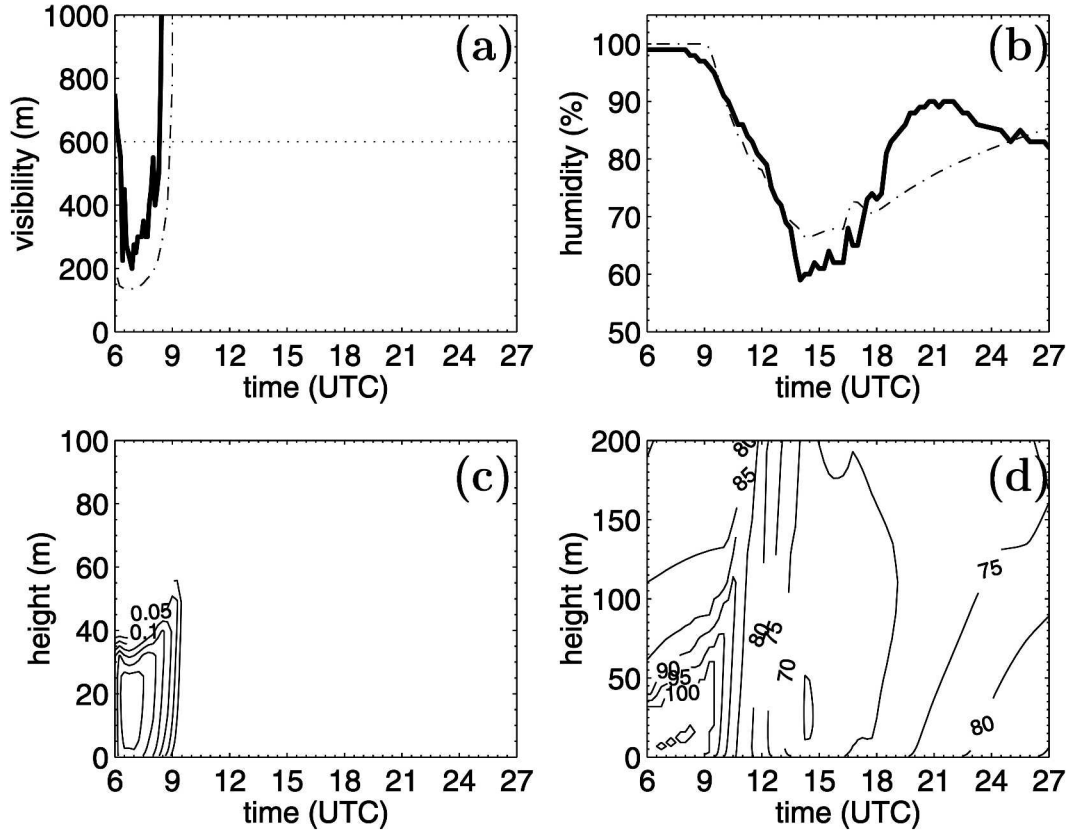


FIG. 14. Case of 3 Mar 2003 at 0600 UTC. Same as Fig. 13, except (c) the contour interval is 0.05 g kg^{-1} .

forecast time for forecasts issued from the local assimilation scheme, from the ALADIN initial conditions, and from persistence. This figure shows that the COBEL-ISBA forecast issued from the local initial conditions is slightly better than the persistence forecast even at very short term (HR is slightly better and FAR is of the same magnitude). These results demonstrate that it does not seem possible to accurately forecast fog and low clouds occurrence without an integrated local observation-assimilation system.

b. Quality of the thermodynamical parameters forecasts

It is now crucial to understand the poorer skill of the forecasts without the local assimilation scheme. The forecast skill of the 2-m temperature is plotted in Fig. 17a for B and in Fig. 17b for the rmse. The simulation without the local assimilation has a strong cold bias of about -4°C during the first hours of the forecast. In opposition, the COBEL-ISBA scheme using local observations does not show much bias ($|B|$ of about 0.2°C , which is of the same order of magnitude as the accuracy of the measurement). This result shows that the local

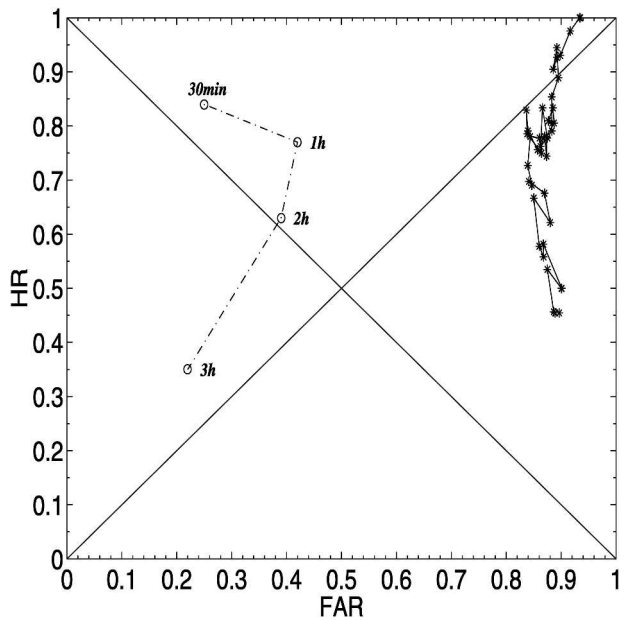


FIG. 15. Comparison of the observed and forecasted LVP conditions for the 2002/03 winter, in an ROC curve format. Same as Fig. 7 for a simulation without the assimilation scheme.

TABLE 3. FBI of the LVP forecast for the simulation with the local assimilation scheme (reference), without the assimilation scheme (initial NWP), and persistence.

	30 min	1 h	2 h	3 h	4 h	5 h	6 h
Reference	1.33	1.47	1.18	1.33	1.51	1.26	1.31
Initial NWP	15.3	15.0	9.16	7.90	8.47	6.77	6.57
Persistence	1.17	1.18	1.00	0.98	1.15	1.02	1.00

assimilation scheme is absolutely essential in producing an accurate forecast of the surface boundary layer structure. The cold bias of temperature could explain the high FBI of the LVP forecast (too many false alarms due to too cold initial conditions).

Concerning the radiative fluxes, the histograms of errors (Fig. 18) clearly show two maxima: one around 0 W m^{-2} and one around -50 W m^{-2} . This illustrates that the low clouds are not well predicted by the ALADIN NWP model and that a correction procedure is crucial in performing an accurate forecast of the radiative cooling. A comparison between the simulations with the local assimilation system (Fig. 12) and with initial conditions issued from the ALADIN model (Fig.

18) shows that the local assimilation scheme clearly reduces the bias on the radiative fluxes (from about -25 to about -10 W m^{-2}). However, a bias still exists in the forecast with the local assimilation scheme, which needs to be eliminated.

6. Influence of the mesoscale flow

The mesoscale flow can strongly influence the evolution of low clouds (e.g., Driedonks and Duynkerke 1989). Our results demonstrate that the mesoscale forcing can be important in performing an accurate forecast of the evolution of low clouds, and this point needs to be explored. This is the main goal of this section. For the simulations presented hereafter, the initial conditions are issued from the local assimilation procedures, and the mesoscale forcing consists of the geostrophic wind, the cloud cover, the horizontal advection of temperature and humidity, and the vertical velocity. This mesoscale forcing is computed from the ALADIN NWP model every 3 h and is linearly interpolated with respect to time. In this section, we focus only on the quality of the LVP forecasts.

In a first stage, the horizontal advections are com-

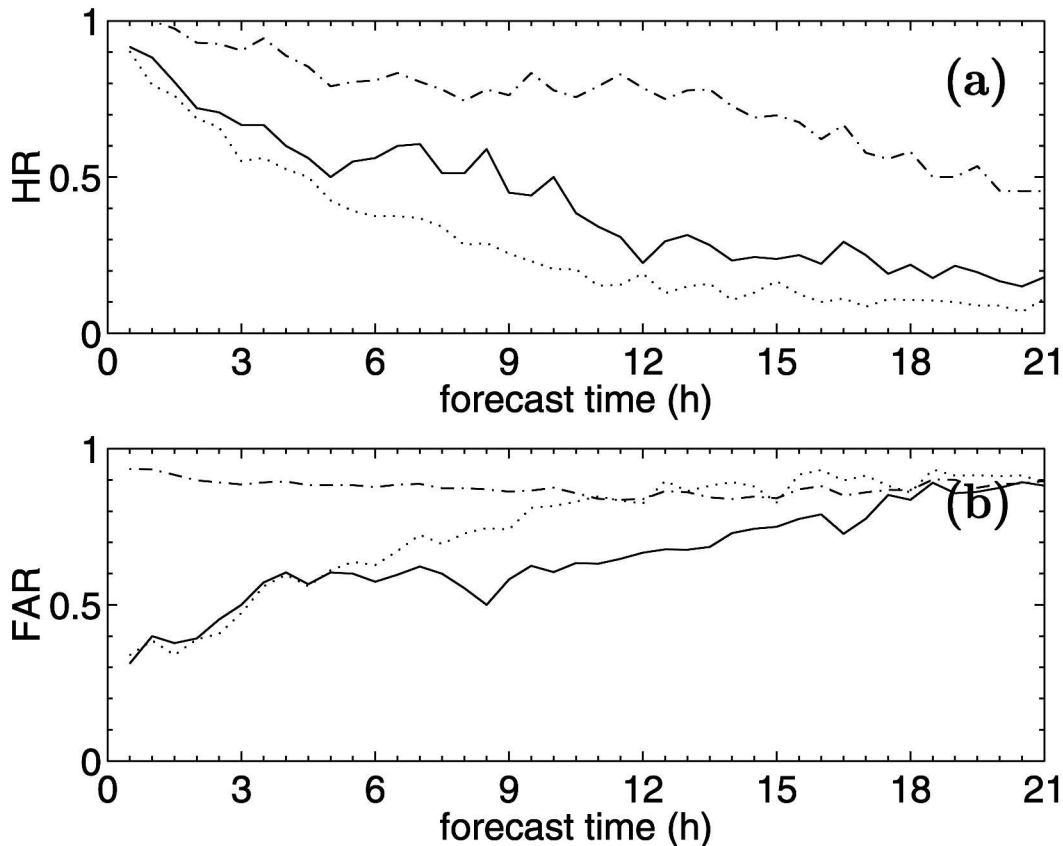


FIG. 16. (a) HR and (b) FAR for a simulation with the local assimilation scheme (solid line), without the assimilation scheme (dashed line), and persistence forecast (dotted line).

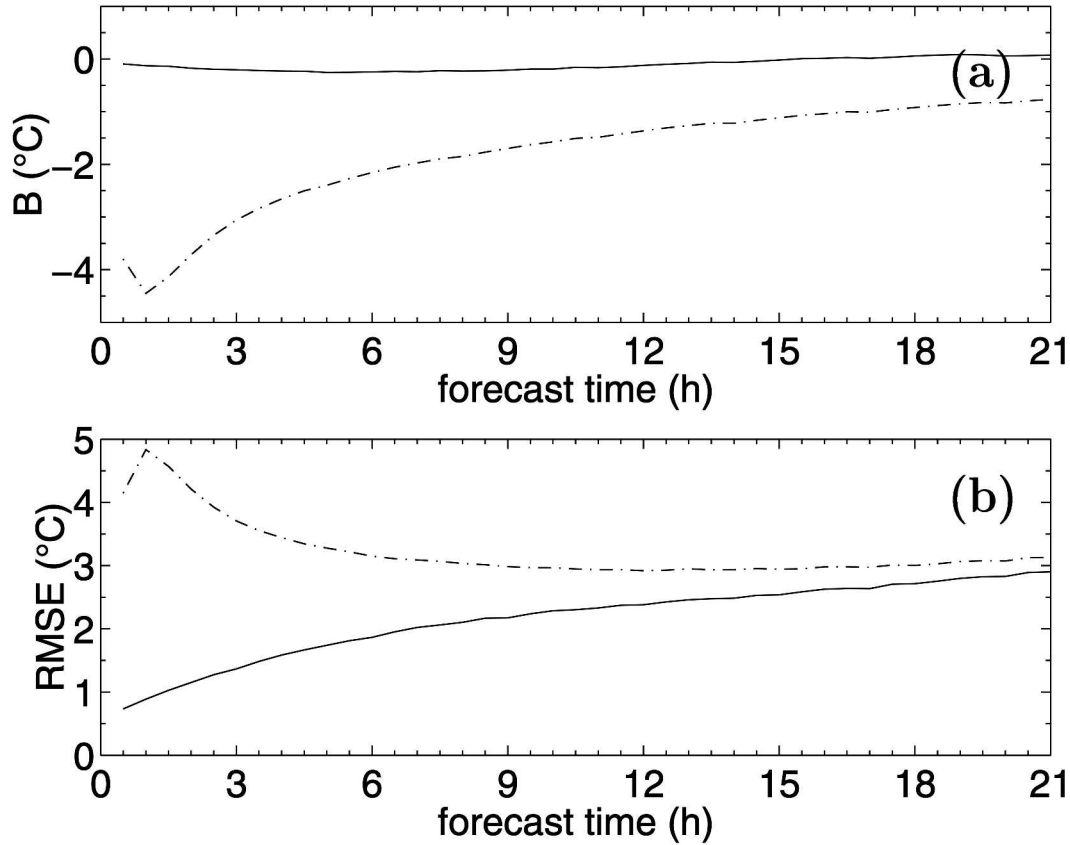


FIG. 17. (a) B and (b) rmse for the 2-m temperature as a function of the forecast time. Simulation with the local assimilation scheme (solid line) and without the assimilation scheme (dashed line).

puted at a horizontal scale of about 20 km. Figure 19 clearly shows that the mesoscale flow from the ALADIN model, computed at small scale, leads to a worsening of the LVP forecast skill during the first 3 h. This is due to a higher number of false alarms (for +1 h forecast, FAR = 51% and HR = 82%, compared to FAR = 40% and HR = 88% in section 4). Afterward, CSI has the same magnitude. This result shows that the ALADIN model does not predict the mesoscale flow accurately enough at the local scale, and consequently no useful information is available at this scale.

However, it can be noticed that the ALADIN fields could be contaminated by small-scale noise [the same kind of problem is also found with the regional Rapid Update Cycle (RUC) model from the National Oceanic and Atmospheric Administration (NOAA); see Roquelaure (2004)]. Therefore, in a second stage, the fields from the ALADIN model have been filtered in order to remove this noise. The horizontal scale of the advection is now roughly 250 km, which is representative of the synoptic scale. Figure 19 shows that this simulation is better than the previous one (in which the

fields are not smoothed). However, the LVP forecast during the first 3 h is always worse than the LVP from section 4. A slight improvement in CSI is observed for LVP forecasts between +9 h and +15 h. But the CSI is always very small at these forecast times (of about 0.2), and one can wonder about the usefulness of this forecast.

To conclude this section, this work has demonstrated that the assumption of horizontal homogeneity can be violated in practice. However, the current NWP mesoscale model cannot give helpful information at the local scale. A 1D model, like COBEL-ISBA, could be especially helpful in forecasting fog when the surface heterogeneity is small, as is the case for Paris-CDG. Under other conditions where heterogeneity is significant (as for the San Francisco or New York airports), it would be perhaps necessary to take into account the mesoscale flow.

7. Conclusions

A new integrated 1D forecast method for fog and low clouds using local observations, a dedicated assimila-

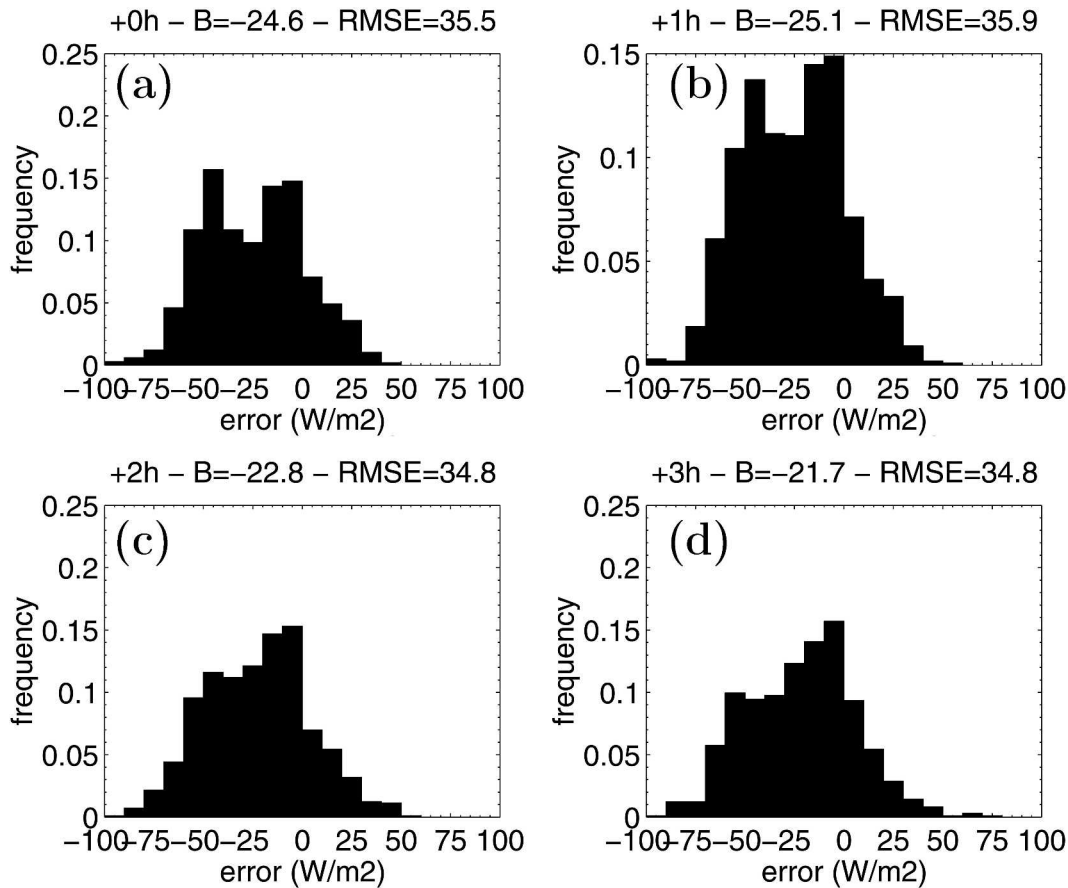


FIG. 18. Distribution of the error on the radiative fluxes at 45 m (W m^{-2}) for the (a) initial conditions, (b) +1 h forecast, (c) +2 h forecast, and (d) +3 h forecast.

tion scheme, and a physically detailed numerical model is described. The main purpose is to produce an accurate forecast of fog and low clouds at a major airport terminal.

We have shown that a 1D model can be an alternative tool for forecasting local parameters, such as visibility, cloud ceiling, and boundary layer parameters. Moreover, this study also reveals that an integrated approach between model and local observations is crucial to improving forecast skill. Precisely, this work indicates that more skillful short-term weather forecasts can be obtained by accurately including boundary layer observations within a detailed boundary layer model. A strong sensitivity to the initial conditions was found, showing that an accurate simulation requires detailed local observations and an accurate local assimilation scheme. For this study, the assimilation scheme follows three steps: estimation of the atmospheric profiles in a 1DVAR framework, correction of atmospheric profiles when fog and/or low clouds are observed, and estimation of soil profiles in order to keep the consistency between the soil profiles and the atmospheric state.

Principally because of the poor quality of the meso-scale flow from the operational ALADIN NWP model (e.g., locally enhanced cold-air drainage flow, clouds), the forecasts of low ceiling and/or poor visibility events are helpful during the first 6 h only. This is the major restriction upon this methodology. The main forecast problem is related to low-level clouds that are very sensitive to the mesoscale flow (particularly subsidence). One hopes that high-resolution satellite imagery, from the new *Meteosat-8* satellite, for instance, could have great potential for improving the forecast skill, by providing useful information on cloud cover. Moreover, mesoscale parameters and surface characteristics could vary in space at the finescale, and it seems that the influence of surface inhomogeneities on fog or low cloud dynamics could be assessed with 3D NWP meso-scale models.

However, further work on the design and evolution of the forecast system presented herein will be required. This study demonstrates that measurements inside the surface boundary layer and radiation fluxes at two levels are absolutely necessary. Single-level obser-

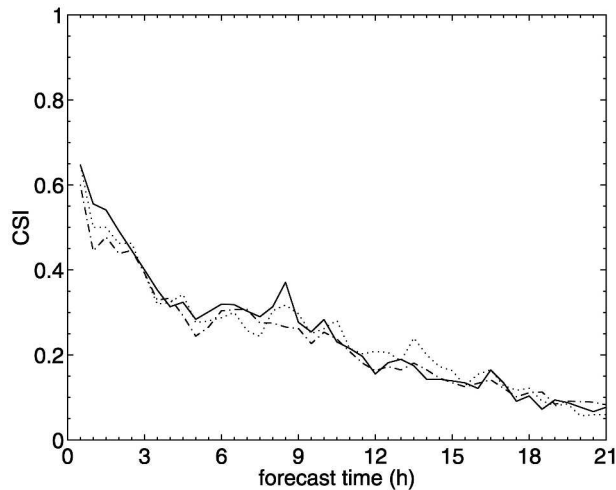


FIG. 19. CSI for a simulation without horizontal advection (solid line), with horizontal advection from no-smoothed field (dashed line), and with smoothed horizontal advection (dotted line).

vations of temperature and humidity are poorly representative of the boundary layer structure (e.g., intensity of the nocturnal inversion). It seems therefore that a careful cost-benefit analysis is necessary to identify whether the money saved by improved forecasts warrants the money spent to construct the observational site (tower, measurement of radiation fluxes at two levels). This cost-benefit analysis will also help us to adjust the forecasting system (ratio of HR to FAR). Once detailed surface boundary layer observations are available, it will be necessary to locally assimilate them. The first version presented in this article used a 3-h assimilation cycle, thus missing many observations (observations are available every 15 min). One way of improve this shortcoming is to discuss the effects of high-frequency assimilations (e.g., every hour) and to illustrate the effects of recent observations on the COBEL-ISBA forecast.

The last but not the least point concerns the predictability of fog and low clouds. Fog and low clouds are small-scale phenomena and have a weak predictability. The LVP forecast is very sensitive to numerous factors, such as the initial conditions and the mesoscale flow. Given the uncertainties of these factors, it is attractive to generate a 1D model ensemble forecast, which will be useful in providing probability forecasts to users. We are convinced that the small scale of the LVP conditions and the number of factors that could possibly affect the forecast make this kind of research highly suitable. Moreover, the definition of probability forecasts will allow the forecast value of the COBEL-ISBA predictions to be measured in terms of the costs and losses

associated with the management of the airport traffic. This point will be the major topic of research for future.

Acknowledgments. We are particularly grateful to the staff of the Paris-CDG meteorological station (and particularly Gilbert Monceau and Daniel Fournier) for their daily help during the field experiment. Daniel Guedalia and Robert Tardif are acknowledged for the discussions around this research and for the work made around the COBEL model. We thank Philippe Lopez and Robert Tardif for helpful comments on the first version of this article. The authors also address special thanks to Florence Habets, Aaron Boone, and Patrick Lemoigne for their friendly help concerning ISBA. Our colleagues from the CNRM/GMME/MC2 team are also gratefully acknowledged for their daily scientific and technical support. And, finally, we would also like to thank the anonymous referees for their relevant comments and criticisms.

REFERENCES

- André, J. C., and L. Mahrt, 1982: The nocturnal surface inversion and influence of clear air radiative cooling. *J. Atmos. Sci.*, **39**, 864–877.
- , J. P. Goutorbe, and A. Perrier, 1986: HAPEX-MOBILHY: A hydrologic atmospheric experiment for the study of water budget and evaporation flux at the climatic scale. *Bull. Amer. Meteor. Soc.*, **67**, 138–144.
- Bechtold, P., 1992: Turbulence et nébulosité dans la couche limite planétaire: Une étude numérique à mésoéchelle. Ph.D. thesis, Université Blaise Pascal, Clermont-Ferrand, France, 188 pp.
- Bergot, T., 1993: Modélisation du brouillard à l'aide d'un modèle 1D forcé par des champs mésoéchelle: Application à la prévision. Ph.D. thesis, Université Paul Sabatier, Toulouse, France, 192 pp.
- , and D. Guedalia, 1994: Numerical forecasting of radiation fog. Part I: Numerical model and sensitivity tests. *Mon. Wea. Rev.*, **122**, 1218–1230.
- , and —, 1996: Evaluation de la qualité de la prévision du brouillard par un modèle numérique. *La Meteorologie*, **14**, 27–35.
- Boone, A. A., 2000: Modélisation des processus hydrologiques dans le schéma de surface ISBA: Inclusion d'un réservoir hydrologique, du gel et modélisation de la neige. Ph.D. thesis, Université Paul Sabatier, Toulouse, France, 252 pp.
- , J. C. Calvet, and J. Noilhan, 1999: The inclusion of a third soil layer in a land surface scheme using the force-restore method. *J. Appl. Meteor.*, **38**, 1611–1630.
- , V. Masson, T. Meyers, and J. Noilhan, 2000: The influence of the inclusion of soil freezing on simulations by a soil vegetation atmosphere transfer scheme. *J. Appl. Meteor.*, **39**, 1544–1569.
- Bougeault, P., and P. Lacarrere, 1989: Parameterization of orography-induced turbulence in a mesoscale model. *Mon. Wea. Rev.*, **117**, 1872–1890.
- Brown, R., and W. T. Roach, 1976: The physics of radiation fog. Part II: A numerical study. *Quart. J. Roy. Meteor. Soc.*, **102**, 335–354.

- Calvet, J. C., and Coauthors, 1999: MUREX: A land-surface field experiment to study the annual cycle of energy and water budgets. *Ann. Geophys.*, **17**, 838–854.
- Chen, T. H., and Coauthors, 1997: Cabauw experimental results from the Project for Intercomparison of Land-Surface Parameterization Schemes (PILPS). *J. Climate*, **10**, 1194–1215.
- Driedonks, A. G. M., and P. G. Duynkerke, 1989: Current problem in the strato-cumulus topped atmospheric boundary layer. *Bound.-Layer Meteor.*, **46**, 275–303.
- Duynkerke, P. G., 1991: Radiation fog: A comparison of model simulation with detailed observations. *Mon. Wea. Rev.*, **119**, 324–341.
- Estournel, C., 1988: Etude de la phase nocturne de la couche limite atmosphérique. Ph.D. thesis, Université Paul Sabatier, Toulouse, France, 176 pp.
- , and D. Guedalia, 1987: A new parameterization of eddy diffusivities for nocturnal boundary layer modeling. *Bound.-Layer Meteor.*, **39**, 191–203.
- Fouquart, Y., and B. Bonnel, 1980: Computations of solar heating of the Earth's atmosphere: A new parameterization. *Beitr. Phys. Atmos.*, **53**, 35–62.
- Guedalia, D., and T. Bergot, 1994: Numerical forecasting of radiation fog. Part II: A comparison of model simulations with several observed fog events. *Mon. Wea. Rev.*, **122**, 1231–1246.
- Habets, F., and Coauthors, 1999: The Isba surface scheme in a macroscale hydrological model applied to the Hapex-Mobilhy area. Part 2: Simulation of streamflows and annual water budgets. *J. Hydrol.*, **217**, 97–118.
- Henderson-Sellers, A., A. Pitman, P. Love, P. Irannejad, and T. Chen, 1995: The Project for Intercomparison of Land Surface Parameterization Schemes (PILPS): Phases 2 and 3. *Bull. Amer. Meteor. Soc.*, **76**, 489–503.
- Kunkel, B., 1984: Parameterization of droplet terminal velocity and extinction coefficient in fog model. *J. Appl. Meteor.*, **23**, 34–41.
- Le Dimet, F. L., and O. Talagrand, 1986: Variational algorithms for analysis and assimilation of meteorological observations: Theoretical aspects. *Tellus*, **38A**, 97–110.
- Musson-Genon, L., 1987: Numerical simulation of a fog event with a one-dimensional boundary layer model. *Mon. Wea. Rev.*, **115**, 592–607.
- Noilhan, J., and S. Planton, 1989: A simple parameterization of land surface processes for meteorological models. *Mon. Wea. Rev.*, **117**, 536–549.
- Pagowski, M., I. Gultepe, and P. King, 2004: Analysis and modeling of an extremely dense fog event in southern Ontario. *J. Appl. Meteor.*, **43**, 3–16.
- Roquelaure, S., 2004: Couplage du modèle COBEL avec le modèle de meso-échelle RUC: Advections horizontales de température et d'humidité. M.S. thesis, L'Université du Québec à Montréal, 113 pp.
- Siebert, J., U. Sievers, and W. Zdunkowski, 1992: A one dimensional simulation of the interaction between land surface processes and the atmosphere. *Bound.-Layer Meteor.*, **59**, 1–34.
- Stull, R. B., 1988: *An Introduction to Boundary Layer Meteorology*. Kluwer Academic, 666 pp.
- Tardif, R., 2004: On the impact of vertical resolution in the numerical forecasting of fog. Preprints, *11th Conf. on Aviation, Range and Aerospace Meteorology*, Hyannis, MA, Amer. Meteor. Soc., CD-ROM, P10.2.
- Vehil, R., J. Monneris, D. Guedalia, and P. Sarthou, 1989: Study of radiative effects (longwave and shortwave) within a fog layer. *Atmos. Res.*, **23**, 179–194.
- Wilson, L. J., and M. Vallee, 2003: The Canadian Updateable Model Output Statistics (UMOS) system: Validation against perfect prog. *Wea. Forecasting*, **18**, 288–302.